NANO LETTERS

LETTER

pubs.acs.org/NanoLett

Roll-to-Roll Anodization and Etching of Aluminum Foils for High-Throughput Surface Nanotexturing

Min Hyung Lee,[†,‡,§,⊥] Namsoo Lim,[∥,⊥,#] Daniel J. Ruebusch,[†,‡,§,⊥] Arash Jamshidi,[†,§] Rehan Kapadia,[†,‡,§] Rebecca Lee,[†] Tae Joon Seok,[†,§] Kuniharu Takei,[†,‡,§] Kee Young Cho,[†,‡,§] Zhiyoung Fan,[†,‡,§] Hwanung Jang,[∥] Ming Wu,[†,§] Gyoujin Cho,[∥] and Ali Javey*[,†,‡,§]

[†]Electrical Engineering and Computer Sciences, University of California, Berkeley, California 94720, United States

[‡]Materials Sciences Division, Lawrence Berkeley National Laboratory, Berkeley, California 94720, United States

[§]Berkeley Sensor and Actuator Center, University of California, Berkeley, California 94720, United States

[∥]Printed Electronics Engineering, Sunchon National University, South Korea

[#]Paru Printed Electronics Research Institute, PARU Co. Ltd. Sunchon, Jeonnam, 540-813, South Korea

Supporting Information

ABSTRACT: A high-throughput process for nanotexturing of hard and soft surfaces based on the roll-to-roll anodization and etching of low-cost aluminum foils is presented. The process enables the precise control of surface topography, feature size, and shape over large areas thereby presenting a highly versatile platform for fabricating substrates with user-defined, functional performance. Specifically, the optical and surface wetting properties of the foil substrates were systematically characterized and tuned through the modulation of the surface texture. In addition, textured aluminum foils with pore and bowl surface features were used as zeptoliter reaction vessels for the well-controlled synthesis of inorganic, organic, and plasmonic nanomaterials, demonstrating yet another powerful potential use of the presented approach.

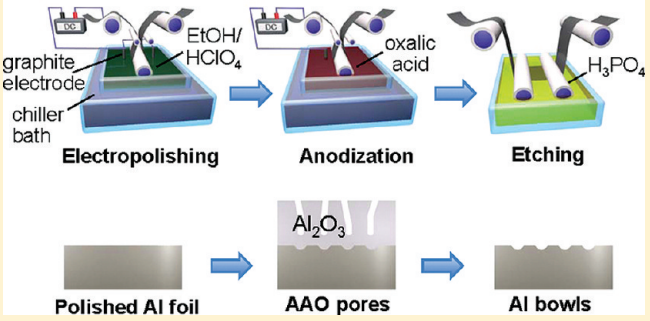

KEYWORDS: Nanopatterning, nanomolding, anodization, anodized alumina, surface texturing

Surface nanotexturing tailors the physical and chemical properties of materials, and has been actively utilized in the past for enabling new functionalities. Selected examples include, antireflective substrates for high-efficiency solar cells,[1,2] superhydrophobic surfaces for self-cleaning materials,[3,4] engineered layers for enhanced or inhibited biofilm formation,[5] low friction surfaces for mechanical systems,[6] and synthetic gecko adhesives.[7,8] In this regard, large-scale (>m^2) production of textured surfaces with optimal micro/nano scale features for a given application is of profound interest, especially for hard substrates such as metals and ceramics. Here, we present roll-to-roll (R2R) anodization and etching of aluminum foils for high-throughput, low-cost nanotexturing of surfaces with tunable topography, and feature size and density. The optical and surface wetting properties of the textured foils were systematically characterized, demonstrating the utility of this technique for enabling substrates with user-defined, functional performance. In addition, R2R textured pores and bowls were used as zeptoliter reaction vessels for the well-controlled synthesis of nanoscale inorganic, organic, and plasmonic materials, demonstrating yet another powerful potential use of the presented platform.

When anodized in an acidic environment with proper process conditions, aluminum oxidizes to form a porous alumina layer consisting of hexagonally packed arrays of nanopores.[9] The pores are normal to the aluminum surface and extend from the surface to the alumina/aluminum interface where there is an oxide barrier layer with near hemispherical geometry. The shape and size of the pores are relatively uniform, with the pitch and diameter being directly proportional to the anodization voltage, and the height controlled by the anodization time. Anodized aluminum oxide (AAO) has proven to be a highly versatile material system that has found important applications in photonics,[10] energy devices including supercapacitors,[11,12] filtration and purification,[13] and architectural and anticorrosive finishes.[14] Furthermore, given the uniformity of size-controlled nanopores, AAO has been widely utilized as a template for ordered synthesis of nanostructured materials, including metallic and semiconductor nanorods,[15,16] nanowires,[17,18] nanotubes[19] and nanoparticles.[20] Importantly, aluminum anodization, in principle, is a highly scalable process as long as a stable voltage and current density are applied with a constant electrolyte temperature and composition. By considering these constraints, here we demonstrate continuous

Received: June 1, 2011
Revised: July 14, 2011
Published: July 20, 2011

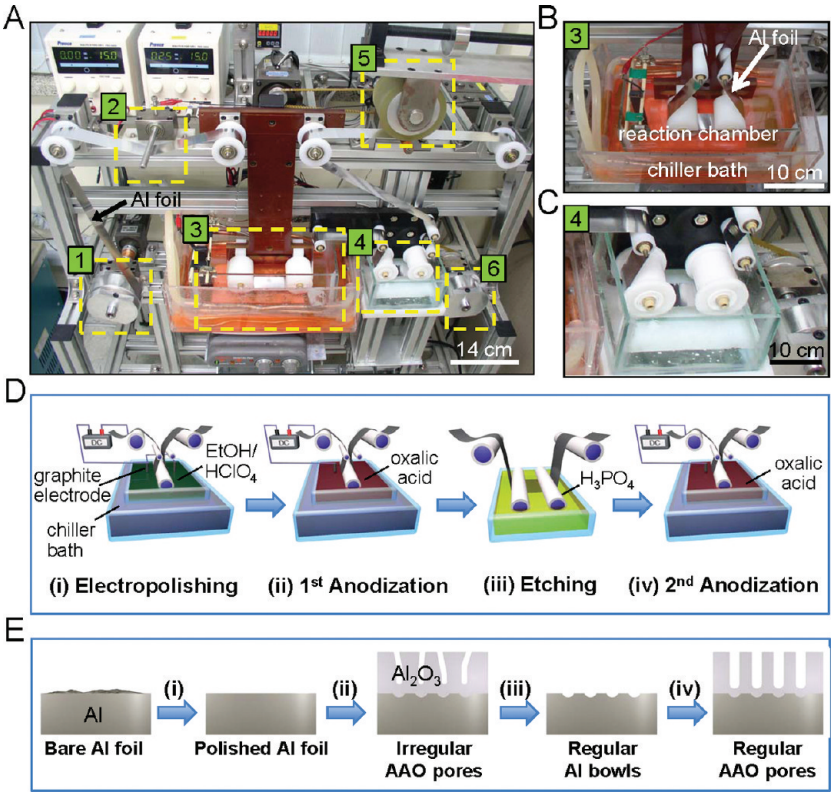

Figure 1. R2R Al texturing system. (A) Optical image of the R2R system used for Al texturization. The important components of the system are highlighted as (1) Al feeding roll, (2) electrical contact to the Al foil, (3) reaction chamber, (4) rinse bath, (5) capstan roll, and (6) rewinding roll. Zoomed-in optical images of (B) the reaction chamber and (C) the rinse bath, respectively. Schematic diagrams of (D) the process and (E) the resulting surface structure after (i) electropolishing, (ii) first anodization, (iii) AAO wet etching, and (iv) second anodization steps used for the fabrication of various surface textures.

R2R nanotexturing of aluminum foils with controlled surface topography over large areas (substrate lengths of ~10 m) by using a combination of anodization and wet etching steps (Figure 1).

Experimental work was performed using a home-built system designed specifically for R2R texturing of aluminum foils (Figure 1A–C). Briefly, a roll of stock aluminum foil (70 μm thick, 3 cm wide, 99.5% pure) is attached to the system and used as the supply roll. The foil travels through a series of rollers until it is guided to the reaction bath, consisting of two nesting pyrex chambers. The outer chamber holds a temperature controlled water bath while the inner chamber consists of the process solution that is continuously stirred to ensure uniformity. Two graphite rods are held in the solution symmetrically about the aluminum foil and serve as the counter electrode while the anodization voltage is directly applied to the aluminum roll. Upon leaving the process solution, the foil is guided to a rinsing deionized (DI) water bath followed by collection at the take-up roll. The system allows for the user-control of both the rolling speed and the line tension.

The R2R texturing process consists of four major steps as depicted in Figure 1D,E: (i) electropolishing of the Al foil to prepare smooth surfaces; (ii) first anodization that initially results in the random nucleation of nanopores on the surface that become ordered beyond a depth of >~500 nm, (iii) selective wet etching of alumina over the Al substrate, resulting in nanobowl surface texturing, and (iv) an optional second anodization step to create ordered nanopores with desired diameter and depth. Each step is performed sequentially using the same R2R system by changing the process solution and rolling speed. To enhance the surface quality and reduce the roughness of Al foil, electropolishing in a 3:1 (v/v) mixture of ethanol and perchloric acid at 20 V was performed (Supporting Information, Figure S1). Smooth surfaces were found to be important for obtaining high quality and ordered surface features during the subsequent anodization processing. The first anodization was carried out in 0.3 M oxalic acid solution at 60 V and bath temperature of 10 °C. The anodized Al foils were subsequently etched by rolling through a mixture of phosphoric acid and chromic acid at 54 °C with a 0.1 mm/s rolling speed (see Supporting Information for details). The purpose of this etch is to strip the irregularly formed nanoporous AAO, resulting in a more ordered dents on the Al surface. At this stage, the substrate consists of uniform nanobowl features. For nanopore texturization, a second anodization step was performed using the same reaction condition as the first anodization.

An optical image of a R2R textured Al foil with a length of ~10 m is shown in Figure 2A. Note that the area of textured surface is not limited to the scale demonstrated here, and can be increased by designing a larger-scale system. Figure 2C–F shows the schematics and scanning electron microscope (SEM) images of Al foils with nanobowl (Figure 2C,D) and nanopore (Figure 2E, F) textures. Al nanobowls obtained from a one-step anodization at 60 V and a subsequent alumina wet etch exhibit an average cross-sectional diameter, $d \sim 95$ nm, depth, $h \sim 75$ nm, pitch, $a_0 \sim 150$ nm, and feature density of $\sim 4.4 \times 10^9$ cm^{-2} (Figure 2D). Alumina nanopores obtained from a two-step anodization

dx.doi.org/10.1021/nl201862d |*Nano Lett.* 2011, 11, 3425–3430

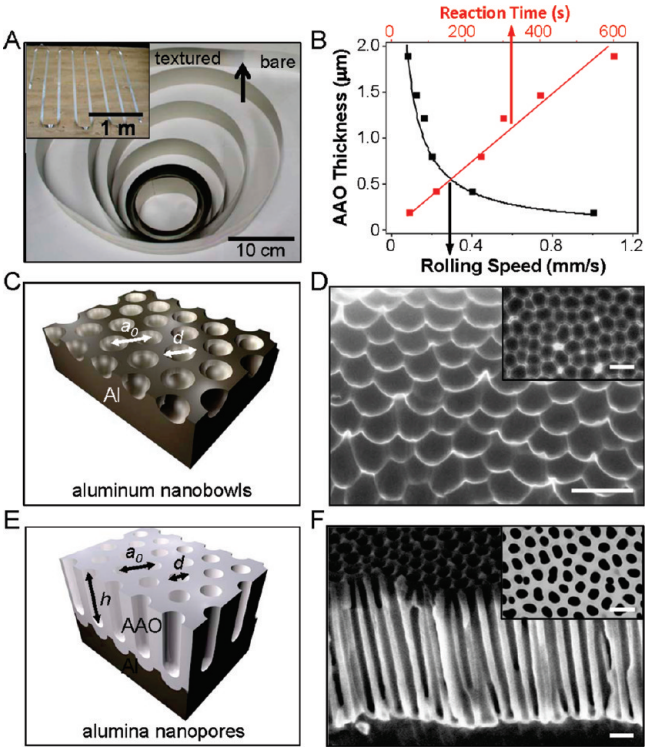

Figure 2. R2R textured Al rolls. (A) Optical image of a large-area Al roll (length of >10 m) prepared by the R2R anodization and etching processes. The arrow marks the borderline for the processed region, where to the left of the arrow the substrate consist of an array of pores over the entire length of the foil. The inset shows the same Al foil in an unrolled configuration. (B) The thickness of the anodized alumina as a function of rolling speed (bottom axis) and reaction time (top axis). (C) Schematic and (D) tilted-view SEM image of an Al foil with nanobowl surface patterns. The inset shows the top-view SEM image of the same sample. (E) Schematic and (F) tilted-view SEM image of alumina nanopores. The top-view SEM image is shown in the inset. The scale bars are 200 nm.

process at 60 V exhibit similar diameter and pitch as the nanobowls with a depth of ~1 μm (Figure 2F) as determined here by a rolling speed of 0.12 mm/s. The nanopore depth (i.e., AAO thickness) as a function of rolling speed and the corresponding anodization time is shown in Figure 2B. The depth is inversely proportional to the rolling speed and is linearly proportional to the reaction time. Note that the reaction time (t_{rxn}) is controlled by the rolling speed (v_{roll}) and is given by $t_{rxn} = L/v_{roll}$, where $L = 48$ mm is the length of the Al foil in the reaction bath. The slope of the pore depth versus reaction time is found to be ~0.2 μm/min which is fast enough for high-throughput manufacturing. The density of surface features can be readily tuned for both topographies by changing the anodizing voltage and solution. For instance, anodization at 195 V in a 150:3:1 (v/v/v) mixture of water, ethylene glycol, and phosphoric acid[1] resulted in the formation of 500 nm pitch bowls and pores with a feature density of $\sim 4 \times 10^8$ cm^{-2} which is approximately 1 order of magnitude lower than those obtained from 60 V anodization (Supporting Information Figure S2). Generally, the pitch is proportional to the anodization voltage which is consistent with the observed results, thereby, presenting good control over the surface feature density. Notably, the diameter of nanopores can be independently tuned by pore widening in phosphoric acid.

Next, we focus on the utility of R2R textured Al foils for practical applications. Given the controlled geometry of the surface features, textured Al foils can be utilized as ideal nanoscale reaction vessels for template-assisted synthesis of nanostructured materials using solution or gas phase processing. To demonstrate this concept, 150 nm pitch nanobowls with 75 nm depth, corresponding to a vessel volume of ~190 zeptoliter, were used as templates for the synthesis of ordered arrays of CdS nanocrystals by discontinuous solution dewetting. Briefly, the textured foil was pulled perpendicularly from a 0.1 M cadmium acetate solution at a withdrawing rate of ~25 μm/s to form single cadmium acetate nanocrystals in each bowl. After drying in the air, the foil was immersed in 1 M sodium sulfide solution for 10 s (ref 21) The process resulted in the formation of individual CdS particles (diameter of 30−40 nm) at well-defined sites (Figure 3A) with the size of the particles being determined by the nanobowl (i.e., reaction vessel) volume. Previous studies have shown that this synthesis technique results in the formation of crystalline particles that could be used for photonic devices.[21] In addition, AAO nanopores were used for the template-assisted, vapor−liquid−solid (VLS) growth[1,18] of Ge nanopillar (NPL) arrays ($d \sim 100$ nm with a length of ~1 μm) as depicted in Figure 3B. Here, Au catalysts were selectively electroplated at the bottom of nanopores, and Ge NPLs were grown in a chemical vapor deposition (CVD) chamber.[18] Template-assisted VLS was previously utilized for the fabrication of NPL photovoltaics,[1] and the large-scale AAO fabrication scheme shown here represents important progress toward the eventual R2R processing of NPL-based modules, especially since R2R CVD has been previously demonstrated.[22]

Textured Al foils may be used as large-area templates for replica molding of functional "soft materials." To demonstrate this concept, polyurethane (PU, Norland 61 optical adhesives) nanodome (Figure 3C) and NPL (Figure 3D) substrates were fabricated by casting and curing PU on bowl and pore templates, respectively. Inverted surface patterns were successfully transferred to the PU substrates with high fidelity. Both surface features have been proposed for substrates with structural antireflective and enhanced light management properties for high-efficiency solar cells, as well as synthetic gecko adhesives.[1,2,7,8] The ability to mass-produce such functional surfaces using a R2R platform, therefore, is of profound technological interest.

The properties of textured aluminum and PU substrates were systematically characterized, first focusing on the wettability and self-cleaning properties. Surface texturing has been widely studied because of its unique physical properties such as tunable wettability,[4,23] reflectivity,[24] and field focusing.[25] Figure 4A shows the water contact angle, θ_{CA} for various surface textures. Fluorocarbons ((tridecafluoro-1,1,2,2-tetrahydrooctyl)trichlorosilane) were vapor deposited on all samples to lower the surface energy and provide a similar surface functionalization for the various samples studied. As a result, the study only highlights the effect of surface topography. The measured contact angle in descending order is for pillars (153°), pores (133°), bowls (126°), and domes (116°), all of which are higher than the bare (i.e., planar) surface (114°). Here, the pitch for all surface textures was fixed at 150 nm. The observed θ_{CA} can be estimated by using Cassie−Baxter and Wenzel models (Figure 4A). Because high-aspect ratio pillars and pores have well-distinguished solid and air interfaces with the water droplet, θ_{CA} is estimated by using Cassie−Baxter model,[26] $\cos \theta_{CA} = f_s \cos \theta_0 + f_a$, where θ_0 is the Young contact angle (i.e., the contact angle of bare substrate), f_s is

dx.doi.org/10.1021/nl201862d |Nano Lett. 2011, 11, 3425–3430

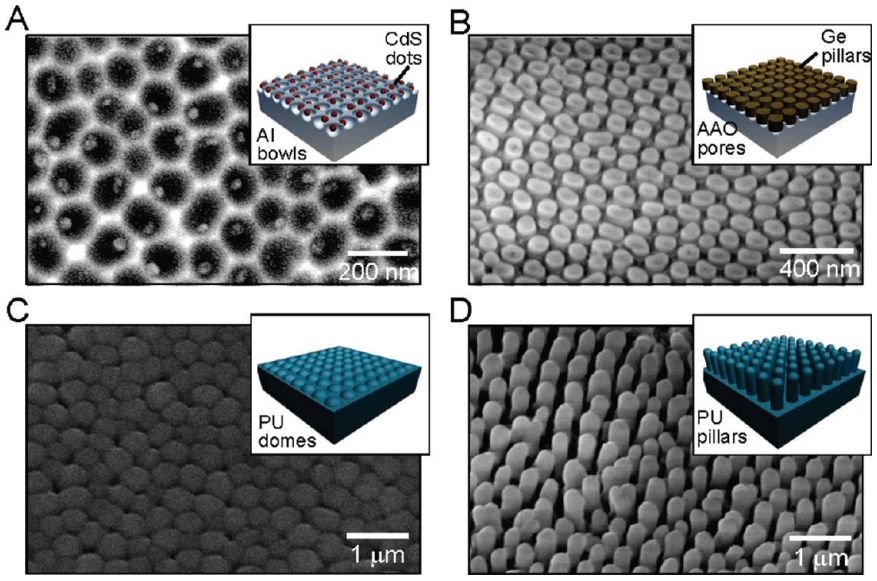

Figure 3. R2R textured Al substrates as nanoscale reaction vessels. SEM images of (A) individual CdS nanocrystals grown in 150 nm pitch Al bowls and (B) Ge NPLs grown in 150 nm pitch AAO pores. (C,D) SEM images of PU nanodomes and PU NPLs fabricated from textured aluminum templates, respectively.

the fractional area of solid−liquid interface, and $f_a = 1 - f_s$ is the fractional area of air−liquid interface. The fractional areas were calculated by $f_s = \pi d^2/2\sqrt{3}(a_0)^2$. The calculated θ_{CA} was 143 and 127° for pillars and pores, respectively, which is in good agreement with the experiments. For bowls and domes, Wenzel model, $\cos\theta_{CA} = r\cos\theta_0$ was used, where r is the surface roughness. The surface roughness was estimated by $r = (\sqrt{3}a_0^2 + 2\pi dh)/\sqrt{3}a_0^2$. The calculated θ_{CA} was 132.7 and 126° for bowls and domes, respectively, which is in qualitative agreement with the experimental observations.

Nanobowl and nanopore surfaces do not exhibit surface self-cleaning properties (i.e, the lotus leaf effect) because the surface indentation induces strong water droplet trapping on the substrate. In contrast, PU NPLs exhibit excellent self-cleaning characteristics (Figure 4B). To demonstrate this concept, 540 nm size silica particles were deposited as dustlike features on the NPL surfaces. By rolling a water droplet on the PU pillars, silica particles were efficiently removed from the surface (Figure 4B). This self-cleaning property demonstrates yet another unique utility of R2R surface engineered substrates.

Another important application of surface texturing is for enhanced and/or tunable photon management. Two specific examples include "moth eye" antireflective coatings and textured back-contacts, both of which have been shown through simulations and preliminary experiments to enhance the absorption and/or carrier collection efficiency of solar cells.[1,27] In this regard, tunable, subwavelength surface texturing is desired over large-areas. Reflectance spectra of bare and textured Al foils are shown in Figure 5A. Bare Al foils exhibit a high average reflectance of ∼40% over the explored wavelength range of 400−800 nm. The light reflectance is dramatically decreased to ∼1% for the 500 nm pitch alumina pores. The low reflectivity of nanopores is attributed to the high refractive index of Al_2O_3 ($n \sim 1.7$) compared to Al ($n \sim 0.8$) and light-trapping in the deep trenches of the pores.[28]

Nanotextured surfaces may also be used as plasmonic substrates for applications including, effective light trapping in thin

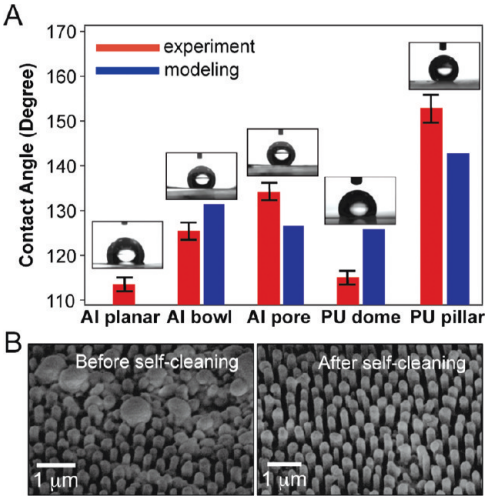

Figure 4. Surface wetting properties of R2R textured surfaces. (A) Contact angle measurement for various texturized surfaces, all functionalized with vapor deposited fluoro carbons. Here, the red bars represent experimental values and the blue bars are the predicted values from theory. (B) SEM images of PU NPLs contaminated with silica beads before (left) and after (right) self-cleaning by rolling a water droplet on the surface.

film photovoltaics, enhanced electromagnetic (EM)-fields for molecular detection[29] and light guiding for plasmonic circuits. Large-area plasmonic substrates with subwavelength pitch are critical for these applications, and in this regard R2R textured substrates are an ideal platform. To demonstrate this concept, 150 nm pitch Au nanohole membranes (∼100 nm thick) were fabricated by evaporating ∼100 nm of Au on the AAOs followed by etching of the Al and alumina layers, and the transfer of the free-standing membranes to glass substrates (Figure 5B). Au nanoholes are conically shaped with small tips which act as "hot-spots" with enhanced EM-fields. As an example system, Au

dx.doi.org/10.1021/nl201862d |*Nano Lett.* 2011, 11, 3425–3430

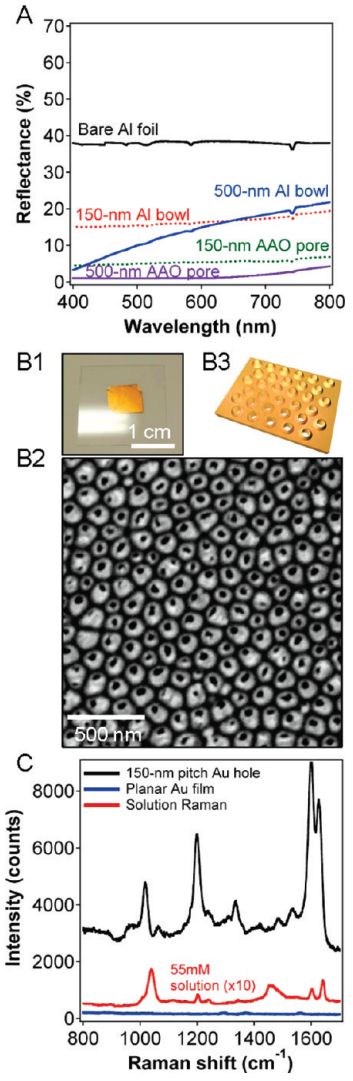

Figure 5. Optical characterization of R2R textured surfaces. (A) Reflectance spectra for bowl, dome, pore, and pillar surface textures. The spectrum for a bare (planar) Al foil is also shown. (B) Optical (B1) and SEM (B2) images and a schematic (B3) of Au nanohole membranes with 150-nm pitch. (C) Surface-enhanced Raman scattering of trans-1,2-bis(4-pyridyl)ethene (BPE) from Au nanohole (black curve) and planar Au (blue curve) substrates. The Raman spectrum (intensity multiplied by 10 for clarity) for a ~50 mM solution of BPE is also shown.

nanohole membranes were functionalized with trans-1,2-bis(4-pyridyl)ethene (BPE) monolayers and excited at a wavelength of λ_{ex} = 785 nm for surface enhanced Raman scattering (SERS) studies (Figure 5C). BPE monolayers were formed on the Au nanohole membranes by soaking the substrates in a 6 mM BPE solution for 2 h, followed by a 2 min rinse with methanol and N_2 drying.[30] Characteristic Raman peaks of BPE at around 1200, 1610, and 1640 cm^{-1} were observed.[30] Au nanohole substrates exhibit a drastic enhancement of Raman signal by ~10^6× over the solution Raman (55 mM BPE) due to the high EM-fields at the tips of the conical holes. By collecting Raman signal using transmission modes with λ_{ex} matched to the surface plasmon resonance of Au holes, an even greater Raman enhancement might be obtained in the future.[29] The proof-of-concept results here demonstrate an easy approach for large-area fabrication of highly desirable plasmonic substrates with engineered feature geometries.

In summary, a versatile R2R process is presented based on the well-established anodization of aluminum foils for the controlled nanotexturing of surfaces over large areas with tunable surface topography, and feature size and density. The surface engineered substrates exhibit functional optical and chemical properties that can be optimized for a given application. In the future, the proposed technology may be used for the fabrication of support substrates for efficient and cost-effective solar cells, self-cleaning surfaces and nanopore supercapacitors, just to name a few examples. Importantly, the textured substrates may be used as nanoscale reaction vessels for the selective synthesis of individual nanomaterials at predefined sites over large areas for fundamental and applied science studies. The scalability of the process can be extended in the future by continuously refilling and exchanging the reagents in the acid bath. In addition, the rolling speed may be increased by using a larger reaction bath and/or a higher reaction temperature. The work presents an important advance in the rapidly growing field of nanomanufacturing.

■ ASSOCIATED CONTENT

Supporting Information. Process details for roll-to-roll electropolishing and anodization; 500 nm pitch nanobowls and nanopores. This material is available free of charge via the Internet at http://pubs.acs.org.

■ AUTHOR INFORMATION

Corresponding Author
*E-mail: ajavey@berkeley.edu.

Author Contributions
⊥These authors contributed equally to this work.

■ ACKNOWLEDGMENT

This work was partially funded by the World Class University program at Sunchon National University, DARPA/DSO, and Mohr Davidow Ventures. The synthesis part of this work was supported by a LDRD from Lawrence Berkeley National Laboratory. A.J. acknowledges a Sloan Fellowship.

■ REFERENCES

(1) Fan, Z.; Razavi, H.; Do, J.-w.; Moriwaki, A.; Ergen, O.; Chueh, Y.-L.; Leu, P. W.; Ho, J. C.; Takahashi, T.; Reichertz, L. A.; Neale, S.; Yu, K.; Wu, M.; Ager, J. W.; Javey, A. *Nat. Mater.* **2009**, *8*, 648–653.
(2) Kelzenberg, M. D.; Boettcher, S. W.; Petykiewicz, J. A.; Turner-Evans, D. B.; Putnam, M. C.; Warren, E. L.; Spurgeon, J. M.; Briggs, R. M.; Lewis, N. S.; Atwater, H. A. *Nat. Mater.* **2010**, *9*, 368–368.
(3) Blossey, R. *Nat. Mater.* **2003**, *2*, 301–306.
(4) Li, X.-M.; Reinhoudt, D.; Crego-Calama, M. *Chem. Soc. Rev.* **2007**, *36*, 1350–1368.
(5) Díaz, C.; Schilardi, P. L.; Salvarezza, R. C.; Fernández Lorenzo de Mele, M. *Langmuir* **2007**, *23*, 11206–11210.
(6) Cottin-Bizonne, C.; Barrat, J.-L.; Bocquet, L.; Charlaix, E. *Nat. Mater.* **2003**, *2*, 237–240.
(7) Geim, A. K.; Dubonos, S. V.; Grigorieva, I. V.; Novoselov, K. S.; Zhukov, A. A.; Shapoval, S. Y. *Nat. Mater.* **2003**, *2*, 461–463.
(8) Ko, H.; Lee, J.; Schubert, B. E.; Chueh, Y.-L.; Leu, P. W.; Fearing, R. S.; Javey, A. *Nano Lett.* **2009**, *9*, 2054–2058.
(9) Masuda, H.; Fukuda, K. *Science* **1995**, *268*, 1466–1468.
(10) Mikulskas, I.; Juodkazis, S.; Tomašiūnas, R.; Dumas, J. G. *Adv. Mater.* **2001**, *13*, 1574–1577.

(11) Banerjee, P.; Perez, I.; Henn-Lecordier, L.; Lee, S. B.; Rubloff, G. W. *Nat. Nanotechnol.* **2009**, *4*, 292–296.
(12) Liang, Y.; Schwab, M. G.; Zhi, L.; Mugnaioli, E.; Kolb, U.; Feng, X.; Müllen, K. *J. Am. Chem. Soc.* **2010**, *132*, 15030–15037.
(13) Vlassiouk, I.; Krasnoslobodtsev, A.; Smirnov, S.; Germann, M. *Langmuir* **2004**, *20*, 9913–9915.
(14) Diggle, J. W.; Downie, T. C.; Goulding, C. W. *Chem. Rev.* **1969**, *69*, 365–405.
(15) Kumar, G.; Tang, H. X.; Schroers, J. *Nature* **2009**, *457*, 868–872.
(16) Lyvers, D. P.; Moon, J.-M.; Kildishev, A. V.; Shalaev, V. M.; Wei, A. *ACS Nano* **2008**, *2*, 2569–2576.
(17) Qin, L.; Park, S.; Huang, L.; Mirkin, C. A. *Science* **2005**, *309*, 113–115.
(18) Ergen, O.; Ruebusch, D. J.; Fang, H.; Rathore, A. A.; Kapadia, R.; Fan, Z.; Takei, K.; Jamshidi, A.; Wu, M.; Javey, A. *J. Am. Chem. Soc.* **2010**, *132*, 13972–13974.
(19) Lee, W.; Scholz, R.; Nielsch, K.; Gösele, U. *Angew. Chem., Int. Ed.* **2005**, *44*, 6050–6054.
(20) Liao, W. S.; Yang, T.; Castellana, E. T.; Kataoka, S.; Cremer, P. S. *Adv. Mater.* **2006**, *18*, 2240–2243.
(21) Barton, J. E.; Odom, T. W. *Nano Lett.* **2004**, *4*, 1525–1528.
(22) Bae, S.; Kim, H.; Lee, Y.; Xu, X.; Park, J.-S.; Zheng, Y.; Balakrishnan, J.; Lei, T.; Ri Kim, H.; Song, Y. I.; Kim, Y.-J.; Kim, K. S.; Ozyilmaz, B.; Ahn, J.-H.; Hong, B. H.; Iijima, S. *Nat. Nanotechnol.* **2010**, *5*, 574–578.
(23) Tuteja, A.; Choi, W.; Ma, M.; Mabry, J. M.; Mazzella, S. A.; Rutledge, G. C.; McKinley, G. H.; Cohen, R. E. *Science* **2007**, *318*, 1618–1622.
(24) Fan, Z.; Kapadia, R.; Leu, P. W.; Zhang, X.; Chueh, Y.-L.; Takei, K.; Yu, K.; Jamshidi, A.; Rathore, A. A.; Ruebusch, D. J.; Wu, M.; Javey, A. *Nano Lett.* **2010**, *10*, 3823–3827.
(25) Fang, Y.; Seong, N.-H.; Dlott, D. D. *Science* **2008**, *321*, 388–392.
(26) Cassie, A. B. D.; Baxter, S. *Trans. Faraday Soc.* **1944**, *40*, 546–551.
(27) Zhu, J.; Hsu, C.-M.; Yu, Z.; Fan, S.; Cui, Y. *Nano Lett.* **2009**, *10*, 1979–1984.
(28) Tian, L.; Ram, K. B.; Ahmad, I.; Menon, L.; Holtz, M. *J. Appl. Phys.* **2005**, *97*, 026101.
(29) Brolo, A. G.; Arctander, E.; Gordon, R.; Leathem, B.; Kavanagh, K. L. *Nano Lett.* **2004**, *4*, 2015–2018.
(30) Fan, J. G.; Zhao, Y. P. *Langmuir* **2008**, *24*, 14172–14175.